Misforecasts of Synoptic Systems: Diagnosis via PV Retrodiction

RENÉ FEHLMANN AND HUW C. DAVIES

Institute for Atmospheric Science, ETH Zu¨rich, Zurich, Switzerland

(Manuscript received 15 August 1996, in final form 16 December 1996)

ABSTRACT

A strategy is outlined to explore the contribution of errors in the specification of tropopause-level flow features to the misforecast of individual synoptic and subsynoptic weather systems. The approach is founded upon a potential vorticity (PV) perspective of the flow. It entails the identification of key upper-level PV error elements at the forecast time, their Lagrangian retrodiction back to the initial analysis time in a process incorporating intermittent PV inversion, and a further forward integration starting from the revised initial state. The procedure can yield direct information on the role and strength of upper-level effects, and if the revised ''forecast'' verifies successfully it can indicate the location and nature of the analysis error.

To illustrate the approach a case study example is provided of a significant misforecast of rapid surface frontal-wave cyclogenesis. A conventional 24-h forecast with a limited-area NWP model failed to capture the low-level cyclone, and the forecast exhibited significant errors in both its low-level and upper-level components of the PV distributions. The revised simulation shadows the analyzed development much more successfully. The result is discussed in the context of the need to improve the initial analysis fields and to devise alternative forecasting strategies.

1. Introduction

Short-range numerical weather prediction of synoptic and subsynoptic features is an event-orientated task. The challenge is to predict for a narrow window in space and time the occurrence or nonoccurrence of specific weather systems, for example, rapid frontal-wave cyclogenesis or a frontal passage with accompanying heavy rainfall. A significant forecast failure can be associated with the development of a nonpredicted system, the nondevelopment of a predicted system, or the inaccurate prediction of the amplitude and/or track of such a system in space and time.

Forecast failure can itself be attributed to deficiencies in the model formulation and/or error in the specification of the initial field. Both shortcomings are compounded by the error growth due to the intrinsic unpredictability of atmospheric flow. Studies of the error growth of medium-range forecasts indicate that there remains significant scope for model improvement (Simmons et al. 1995) and that initial conditions can also play a crucial role (Molteni et al. 1996). Studies of the error characteristics of short-range forecasts need to take into account the event-orientated and short-range nature of the prediction task and thereby recognize that the error growth need be neither spatially diffuse nor temporally sustained. In effect, localized transient growth, unrelated to the standard Lyapunov rate, might frequently dominate the error evolution.

The extant studies on error growth in short-range forecasts have followed several avenues. Predictability experiments with limited-area models have documented the sensitivity of the domain-averaged error measures to the lateral boundary data and the structure of the initial perturbations–error fields (e.g., Errico and Baumhefner 1987; van Tuyl and Errico 1989; Vukicevic 1991; Lüthi et al. 1996). Simulations of individual events have provided some indication of the influence of spatial resolution, parameterization schemes, and initial analysis errors (see, e.g., Kuo and Reed 1988; Mullen and Baumhefner 1989; Shutts 1990). Likewise, the COMPARE project (see, e.g., Gyakum et al. 1995) intercompares the performance of different operational forecast models. Results from this project, derived for an event of secondary cyclogenesis, indicate a sensitivity to horizontal resolution, a tendency to underestimate the deepening and to slightly misrepresent the track, and also an important contribution of upper-level features to the cyclone's initiation. An alternative approach to the problem is to exploit the adjoint of a limited-area forecast model to investigate the sensitivity to errors in the initial state and to ascertain the structure and growth rate of the associated singular vectors (Errico and Vukicevic 1992; Errico et al. 1993; Ehrendorfer and Errico 1995; Langland et al. 1995). The results suggest that the optimal structures for growth correspond to shallow lower-tropospheric perturbations that slope upstream with

Corresponding author address: Dr. René Fehlmann, Atmospheric Physics, HPPL6, ETH Honggerbeg, CH-8093 Zurich, Switzerland.
E-mail: fehlmann@atmos.umnw.ethz.ch

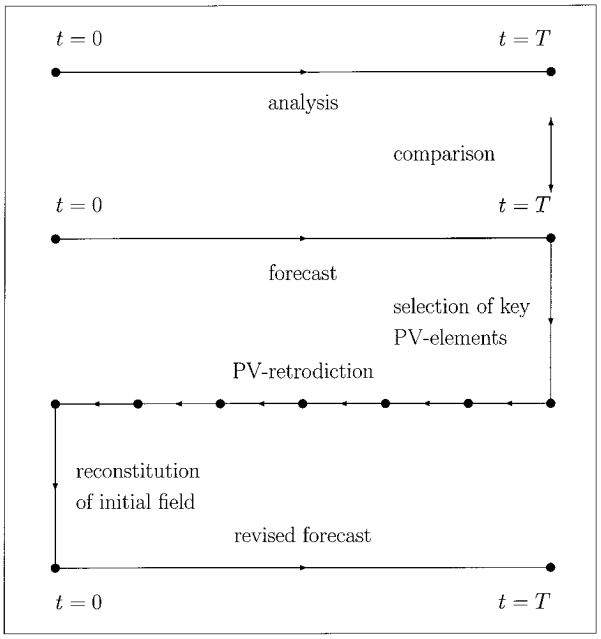

FIG. 1. A schematic of the four-step PV-retrodiction cycle. It comprises (i) a comparison of the analysis and the standard forecast and selection of key upper-level PV error elements at $t = T$, (ii) a Lagrangian advection of these elements back to the initial time in a process involving intermittent PV inversion to successively modify the analyzed fields, (iii) an incorporation of the resulting PV distribution at $t = 0$, and (iv) a further conventional foreward prediction with the revised fields.

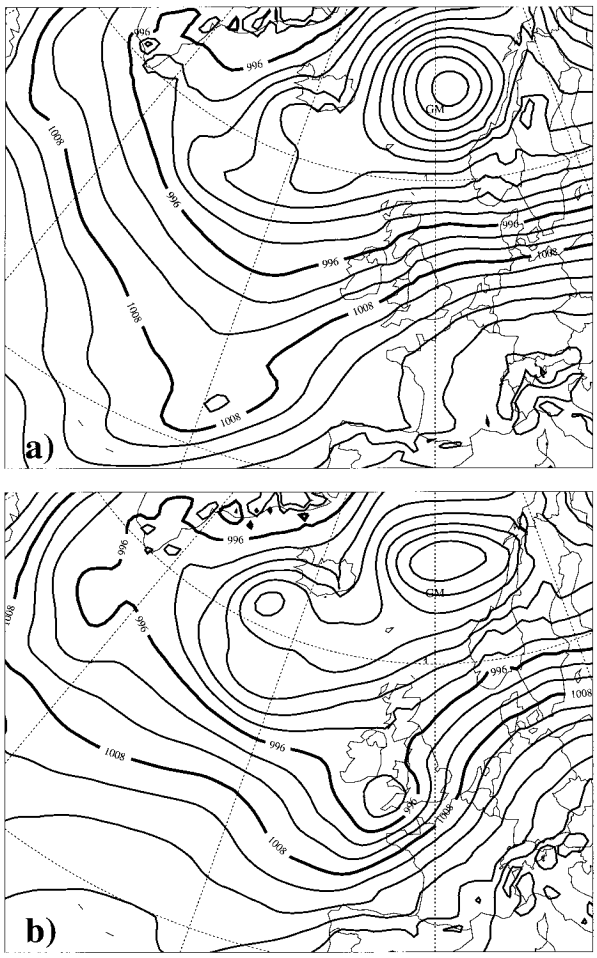

FIG. 2. The sea level pressure pattern (spacing 4 hPa, 996- and 1008-hPa isolines bold) for 0000 and 1200 UTC 13 January 1993.

height. Caveats to this approach relate to the limitations of the tangent-linear model and the sensitivity of the perturbations to the choice of the error norm. Another conceivable approach would be to examine consecutive operational forecasts during their (inevitably short) overlapping integration periods.

The focus of this study is the diagnosis of the initial errors in short-range forecasts. Such a diagnosis should ideally help elicit the nature, cause, and/or origin of the associated error(s) and point to the requisite remedial action. For NWP forecast systems, the errors in the initial analysis stem from the combination of errors in the background fields derived from an earlier forecast and an inadequate observational dataset.

Deficiencies in the analysis can be related to, and interpreted in terms of, errors in the location of key upper- and lower-level flow features and to the richly structured subsynoptic-scale features of the precursor flow. Moreover, the projection of these errors onto the singular vectors will determine the form and amplitude of the subsequent error growth. A recent approach (Rabier et al. 1996) has been to adapt the adjoint approach to examine the sensitivity of the 48-h forecast errors with respect to the initial analysis.

Here an alternative approach is pursued to diagnose the contribution of tropopause-level flow features to misforecasts. The strategy, based upon the potential vorticity (PV) perspective, is outlined in the next section. It can yield information on the nature of the PV error in the initial analysis and insight on the dynamics of the error evolution. Its use is illustrated by application to a misforecast of an event of frontal-wave cyclogenesis (section 3). In light of the derived results, some comments are made on more general analysis, predictability, and forecasting issues (section 4).

2. The approach

The PV perspective of synoptic and subsynoptic-scale atmospheric flow is founded on three consituents: PV conservation in the adiabatic and frictionless limit, PV inversion in the balanced-flow limit, and PV partition into coherent, distinctive elements of the observed flow. The approach to be outlined here utilizes all three constituents.

First, the concept of partition encourages the identification of cyclogenesis with the self-development and the strong interaction of key PV elements. These elements are taken to be major undulations and fragments

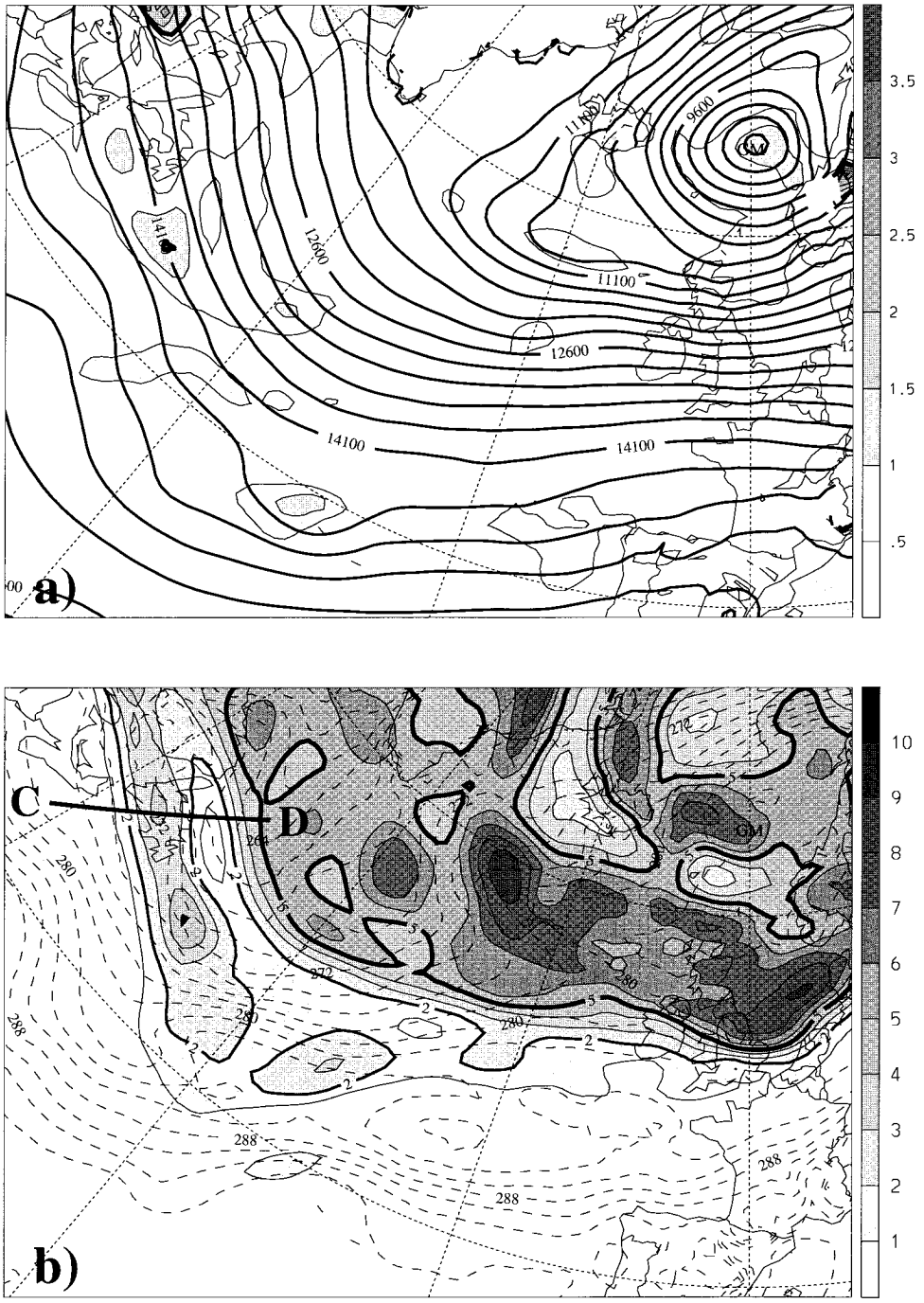

FIG. 3. ECMWF initialized analysis at the starting time of the forecast (i.e., 1200 UTC 12 January). (a) Geopotential at 850 hPa (thin line, spacing 300 m^2 s^{-2}) and potential vorticity (shaded, spacing 0.5 PVU, the thick line denotes the l.5-PVU isoline). (b) Potential temperature field at 850 hPa (dashed lines, spacing 2 K) and potential vorticity on the 310-K isentropic surface (shaded, spacing 1 PVU). Contour spacing is 2 K for potential temperature and 1 PVU for potential vorticity. (The thick line corresponds to the 2-PVU isoline and the bold to the 5-PVU isoline.)

of the potential vorticity on tropopause-transcending isentropic surfaces, elongated subsynoptic prefrontal bands of low-level potential vorticity, emerging towers of potential vorticity in the neighborhood of the incipient cyclone, and the surface potential temperature pattern that accompanies fronts. [For an account of the nature of the various possible cyclogenetic interactions see Hoskins et al. (1985), Hoskins and Berrisford

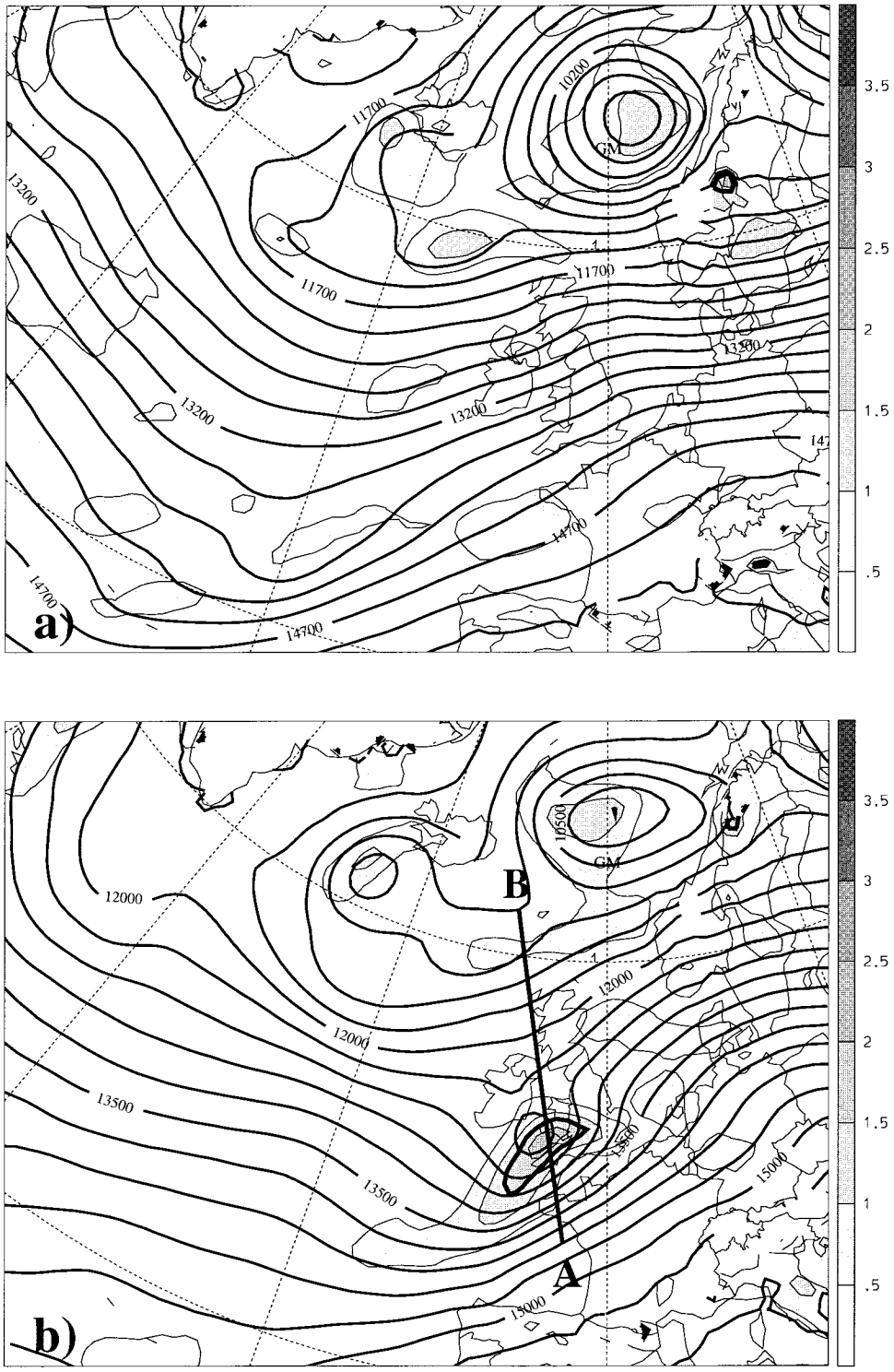

FIG. 4. ECMWF initialized analysis fields on the 850-hPa surface for (a) 0000 UTC 13 January 1993 and (b) 1200 UTC 13 January 1993. The displayed fields are geopotential and potential vorticity (same spacing as in Fig. 3a). The bold line demarks the location of the vertical section shown in Fig. 6.

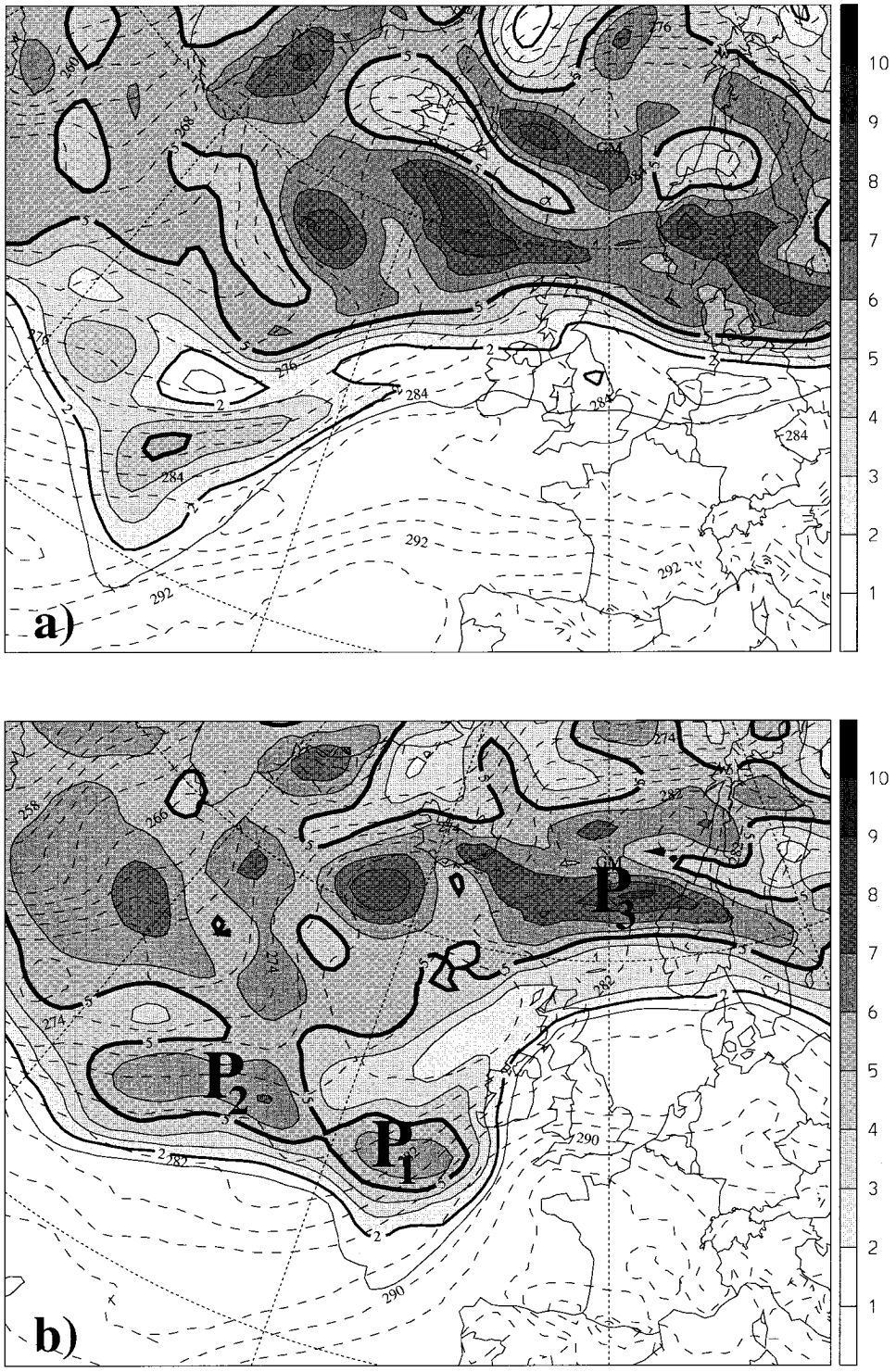

FIG. 5. ECMWF initialized analysis fields for (a) 0000 UTC 13 January 1993 and (b) 1200 UTC 13 January 1993. The displayed fields are potential temperature (dashed lines) on 850 hPa and potential vorticity (shaded) on the 310-K isentropic surface (same spacing as in Fig. 3b).

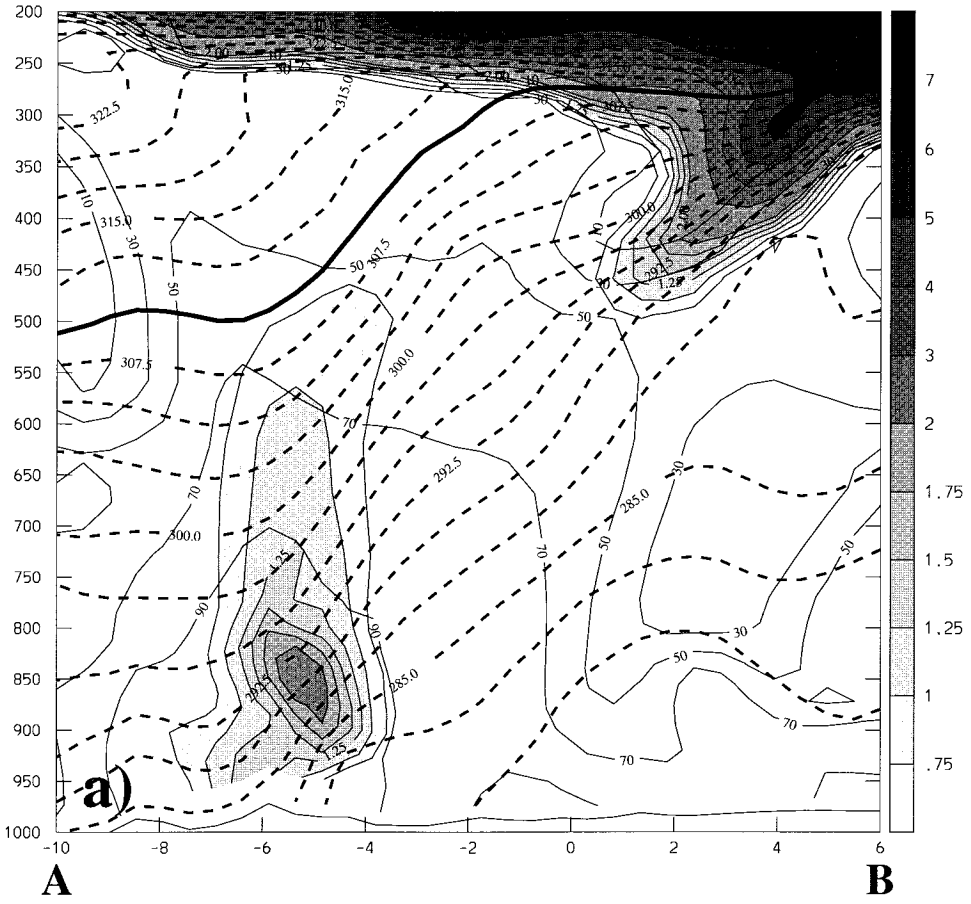

FIG. 6. Cross section at 1200 UTC 13 January along the line indicated in Fig. 4. The displayed fields are (a) PV (shaded, spacing 0.25 PVU for values less than or equal to 2 PVU and 1 PVU for values greater than or equal to 2 PVU), potential temperature (dashed lines, thick line indicates 310 K, spacing 2.5 K), and relative humidity (thin lines, spacing 20%); (b) diabatic heating rate (shaded, spacing 0.5 K h^{-1}), diabatic PV rate (positive values solid lines, negative values dashed lines, spacing 0.1 PVU h^{-1}, zero line omitted), and superimposed are the 1-PVU and 2-PVU isolines (dash–dotted lines).

(1988), Schär and Davies (1990), Joly and Thorpe (1990), Thorncroft and Hoskins (1990), Davis and Emanuel (1991), Reed and Stoelinga (1992), Malardel et al. (1993), and Appenzeller and Davies (1996).] Pivotal to the present study is the deduction that in the ambient environment of incipient cyclogenesis the omission of one feature, or the misspecification of its amplitude or location (and thereby its phase relative to the other key PV signatures), can have a major impact upon the subsequent development.

Second, the principle PV conservation can be applied to anomalously positive PV elements at tropopause level since, for these stratospheric in origin features, the in situ diabatic and frictional effects are comparatively weak. (This clearly does not apply to mid- and low-tropospheric PV elements that often owe their very existence to cloud-diabatic effects.) In effect these elements are/were advected quasi-conservatively by the flow field.

Third, the concept of inversion (together with retrodictive advection) provides an estimate of the space–time history and the associated flow field of these tropopause-level PV elements.

The proposed diagnostic strategy utilizes these three constituents of PV perspective to examine a misforecast and entails four sequential steps (see Fig. 1):

1) the identification of key upper-level PV error elements at the forecast time by comparison with the contemporaneous analysis;
2) the Lagrangian retrodiction of these elements back to the initial time in a process involving intermittent PV inversion to successively modify the advective component of the analyzed (or model forecast) flow fields;
3) incorporation of the resulting PV distribution at the initial time to form a revised initial analysis; and
4) a further conventional forward prediction with the revised fields.

[In step 2 the back trajectories are evaluated using

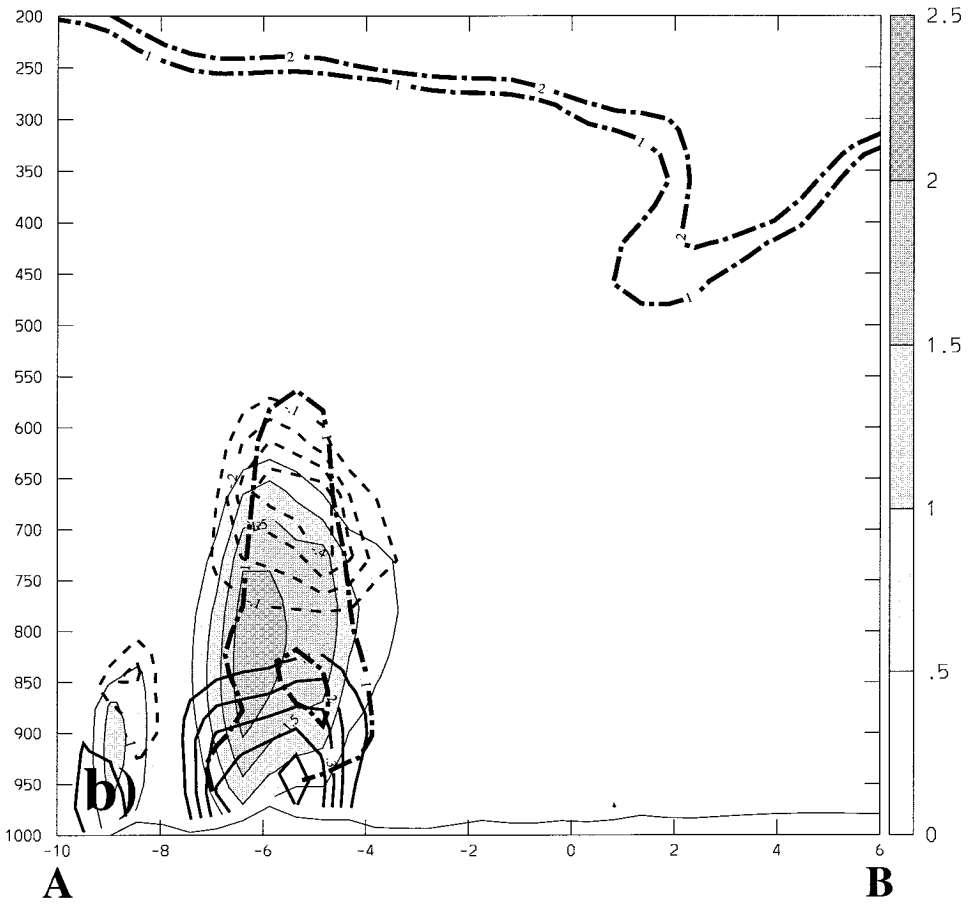

FIG. 6. (*Continued*)

the procedure documented in Wernli and Davies (1997), and the PV inversion is performed by applying an iterative procedure to an approximate form for the potential vorticity relation. The accuracy of the latter scheme can be, and is, monitored by recomputing the full potential vorticity from the derived fields.]

This four-step procedure isolates the contribution of the upper-level PV error. It has therefore the potential to provide information on the nature of the error in the initial field and to yield insight on the role of upper-level effects in the cyclogenesis.

3. A case study

To illustrate the foregoing approach we apply it to a misforecast of one particular event of rapid Atlantic frontal-wave cyclogenesis in January 1993. The analysis data are derived from the 6-h ''forecast-cum-analysis'' cycle of the European Centre for Medium-Range Weather Forecasts (ECMWF). The Centre's T213/L31 operational model has an effective horizontal resolution of approximately 70 km in midlatitudes and a vertical resolution at tropopause levels of about 25 hPa (Simmons 1991).

Simulations of the event are performed with a version of the so-called Europa model (EM)—the limited-area weather prediction model of the German weather service [for details of the model formulation and parameterization schemes see Majewski (1991)]. The model operates with a rotated coordinate system and delivers a horizontal resolution of 0.5° (about 55 km in the North Atlantic); for this study, it was operated with 32 levels in the vertical. The model's integration domain encloses most of western Europe and the North Atlantic, and at the lateral boundaries the simulated fields are relaxed to those of the ECMWF analysis.

a. Synopsis of the analyzed event

The genesis of the frontal-wave cyclone occurred in the 24 h from 1200 UTC 12 January 1993. The system originated on an elongated cold front that trailed out from Europe to the mid-Atlantic. Figure 2 shows the sea level pressure (SLP) pattern for 0000 and 1200 UTC 13 January. The system is discernible at the earlier time (Fig. 2a) and intensified rapidly in the 6-h period to 1200 UTC to yield a tight mesoscale low pressure system off the South Wales coast (Fig. 2b). A detailed

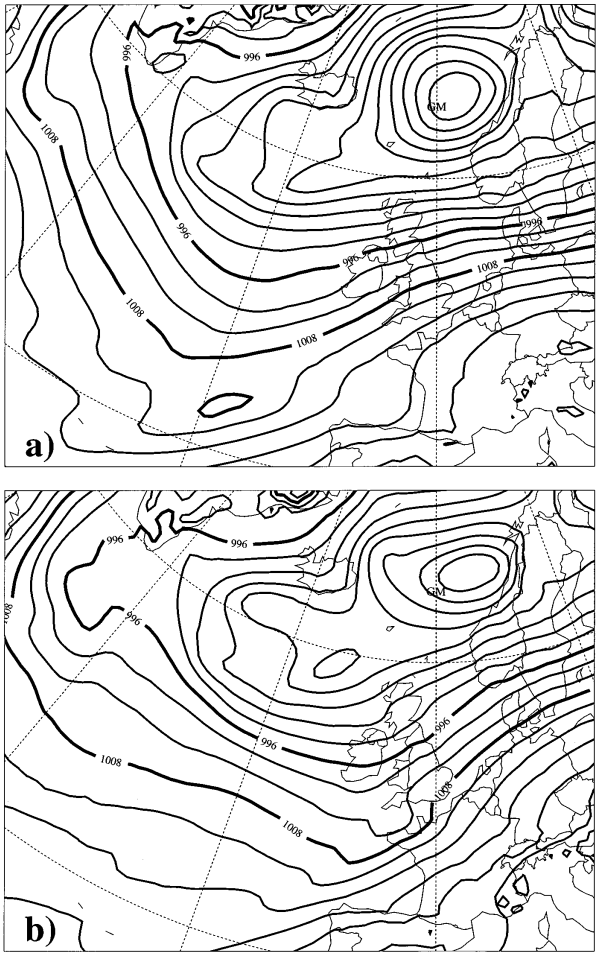

FIG. 7. As for Fig. 2 but now derived from the EM forecast.

analysis recording the synoptic, satellite, radar, and PV signatures of the event is given by Browning and Roberts (1994). Here a synopsis is given of features that are particularly pertinent to the present study.

At the starting time for the forecast—1200 UTC 12 January—the analysis shows that at 850 hPa there is a slack mid-Atlantic trough with a weak PV anomaly at its base (Fig. 3a). Also at this time there are hints of almost collocated undulations in the 850-hPa thermal field and upper-level PV pattern (Fig. 3b). The corresponding fields at 0000 and 1200 UTC 13 January (see Figs. 4 and 5) show synchronous development of upper- and lower-level features. By 1200 UTC 13 January there is, at 850 hPa, a distinct mesoscale trough with a collocated thermal ridge and a strong mesoscale arch of potential vorticity, while aloft on the 310-K isentropic surface there has emerged a compact quasi-circular subsynoptic PV feature (labeled P_1 in Fig. 5) to the west of the low-level system.

Further details of the strength and structure of the system's PV anomalies at 1200 UTC 13 January are shown in the cross sections displayed in Fig. 6 (location of the section is marked in Fig. 4b). A diabatic-induced tropospheric PV tower extends to 500 hPa, with its maximum (~1.5 PVU) located just below the 850-hPa level. The tower's diabatic heating rate and PV production rate at this time (computed following Wernli and Davies 1997) possess maxima of, respectively, 2 K h^{-1} at 800 hPa and 0.5 PVU h^{-1} at 950 hPa. These patterns are consistent with the continuous production and subsequent destruction of potential vorticity of the air parcels as they transit through the tower (cf. Wernli and Davies 1997). The stratospheric PV intrusion aloft has an amplitude of about 7 PVU and reaches down to circa 450 hPa in a region that is essentially devoid of diabatic effects.

From a PV perspective, the tower and the intrusion contribute substantially to determining the depth and location of the associated surface cyclone. Thus, the accurate representation of the structure and amplitude of these features is requisite for a successful forecast. Finally note that at 1200 UTC 13 January the sytem's upper- and low-level features are suitably phased for continued development, and indeed in the subsequent 24 h the depression deepened a further 20 hPa.

b. A forecast

A 24-h forecast from 1200 UTC 12 January performed with the EM model and starting from the initial analysis fields of the ECMWF fails to capture the cyclogenesis.

Comparison of the evolution of the forecasted fields (Figs. 7–9) with the corresponding analysis fields (Figs. 2, 4, 5) reveals only modest differences at 0000 UTC 13 January, but the differences amount to a significant misforecast by 1200 UTC. At the latter time the SLP field shows only a weak cyclone, and likewise at 850 hPa the geopotential and potential temperature fields exhibit much weaker and more southerly undulations than those of the analysis. In the forecast fields the tropospheric PV signal is much less pronounced, and the upper-level PV pattern is less structured and weaker (approximately 3 PVU compared with 7 PVU in the analysis field).

c. Application of the approach

The first task—step 1—is to identify key upper-level PV error elements at the forecast time. Coinspection of the forecasted and analyzed PV patterns on the 310-K isentropic surface for 1200 UTC 13 January (Figs. 5b and 9b) indicates that two analyzed anomalies (labeled P_1 and P_3 in Fig. 5b) are absent from the forecast field, while a third (labeled P_2) is much too weak. This is further highlighted in Fig. 10a, which shows the corresponding difference—hereafter termed somewhat loosely the PV error.

The error associated with P_1 is unipolar and localized, that of P_2 is unipolar but somewhat weaker and more

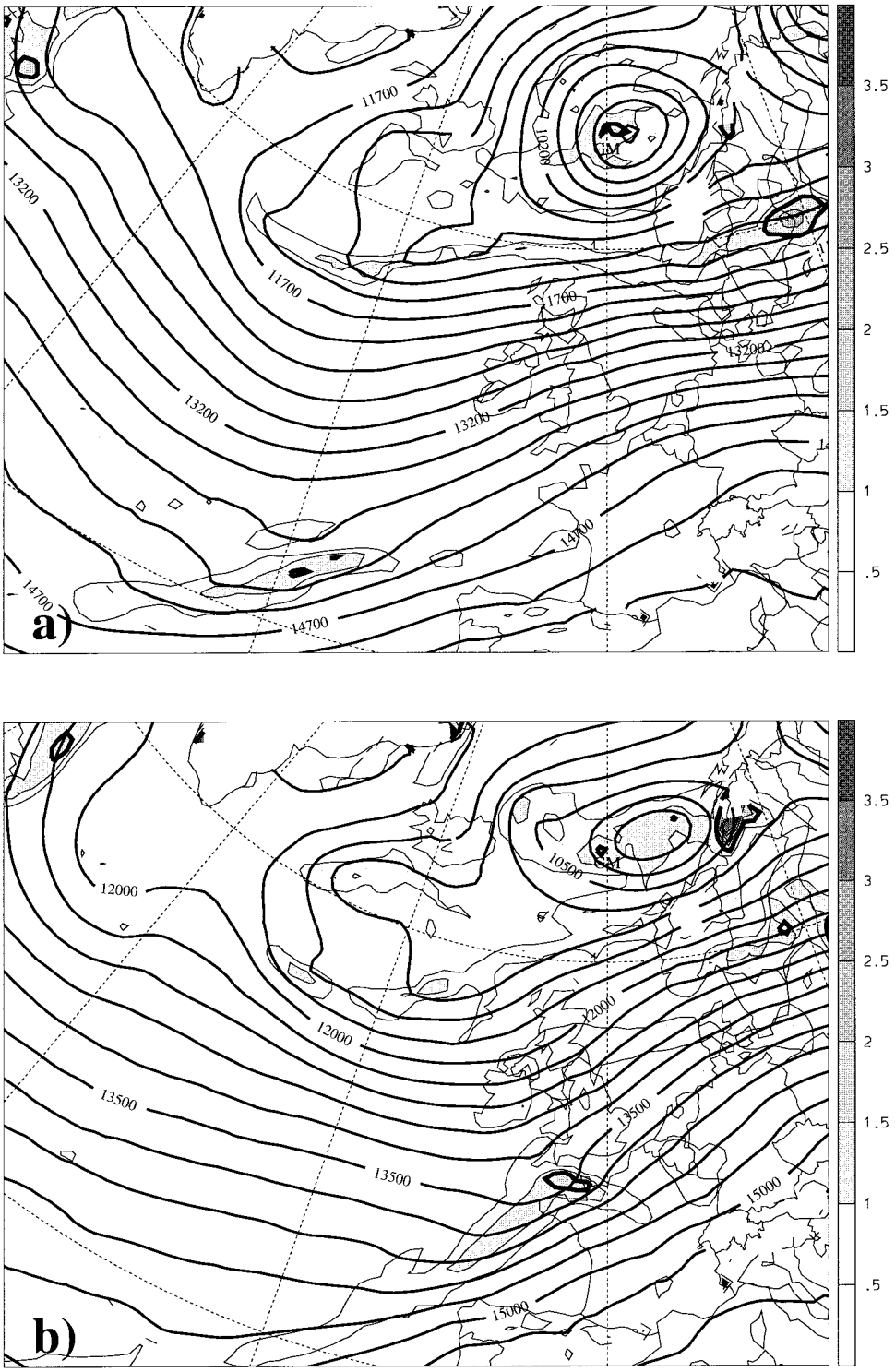

FIG. 8. The analog of Fig. 4 but now derived from the forecast with the EM model.

diffuse, whereas that associated with P_3 is dipolar and more complex. The unipolar and dipolar error types are suggestive, respectively, of an undetected PV anomaly and of a mislocated PV anomaly. The inference regarding P_1 is supported by inspection of a succession of analyzed isentropic charts that reveal the nonconservation of its amplitude (cf. Figs. 3b and 5). The misrepresentation of the P_1 anomaly contributes directly to

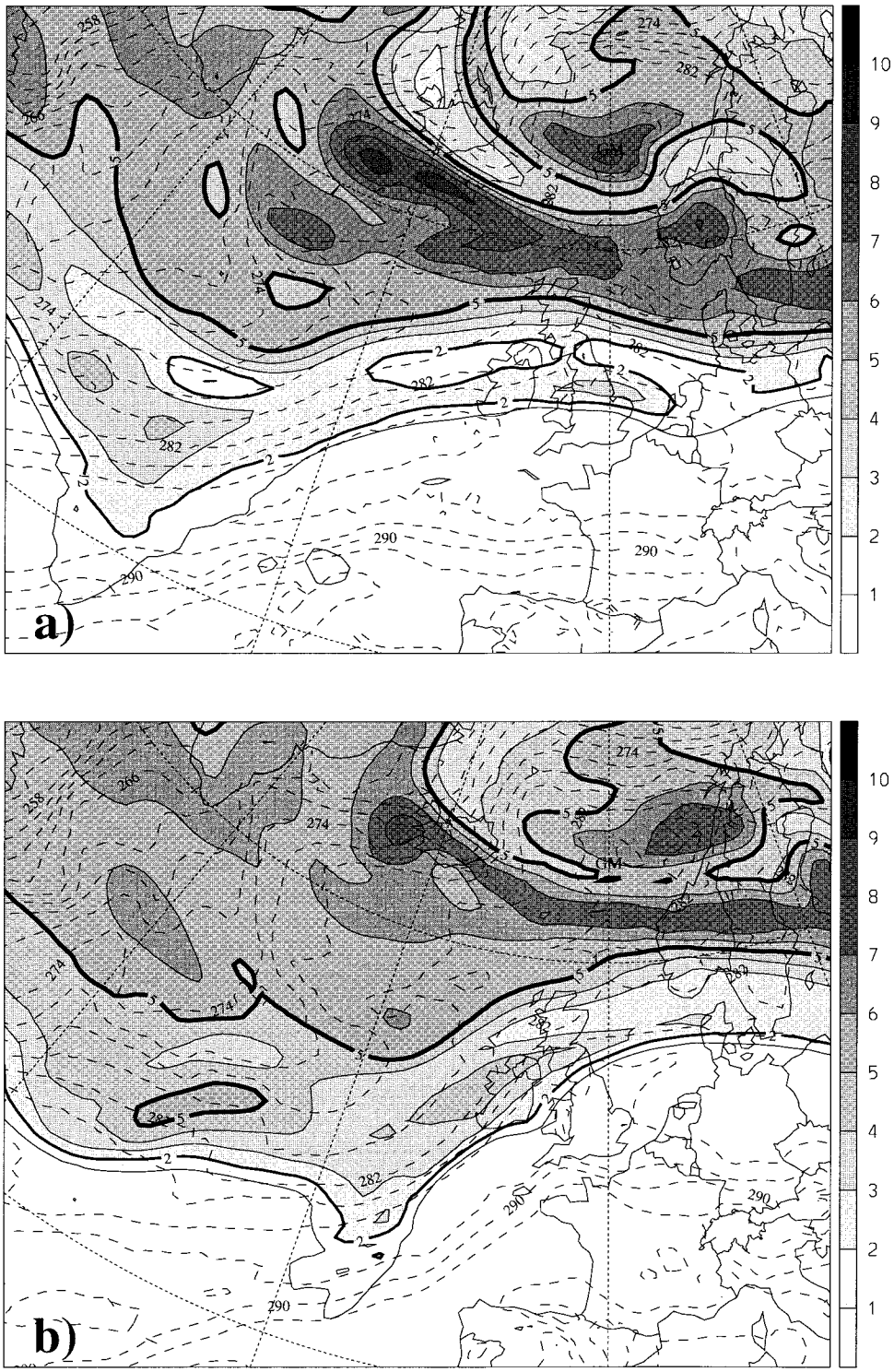

FIG. 9. The analog of Fig. 5 but now derived from the forecast with the EM model.

the misforecast of the structure and strength of the surface cyclone, and the misplacement of P_3 to a location closer to the evolving cyclone could have influenced the latter's track and ascent field.

For step 2, two three-dimensional envelopes are established that fully encompass the spatial domains demarked by large PV errors associated, respectively, with the P_1 and P_3 anomalies. These envelopes are then re-

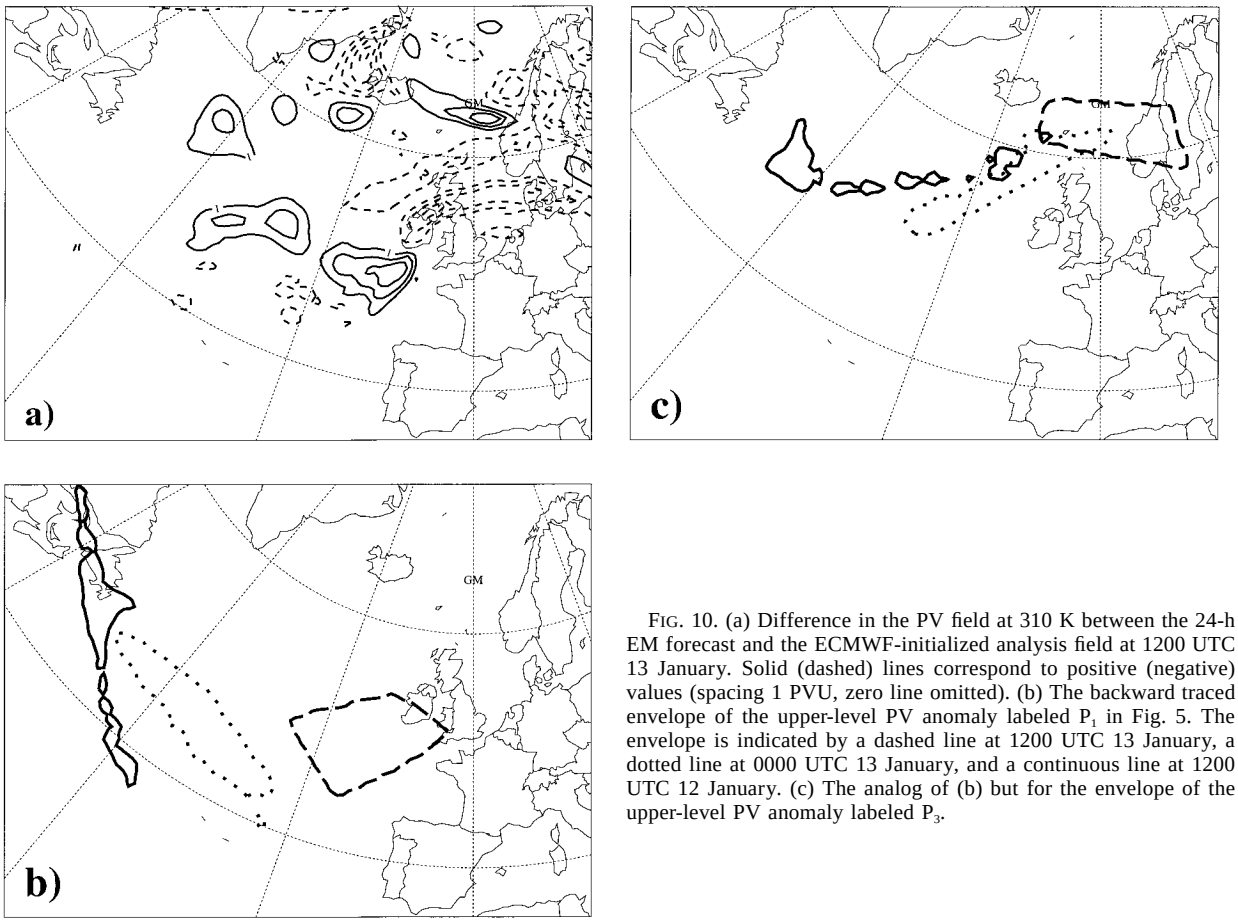

FIG. 10. (a) Difference in the PV field at 310 K between the 24-h EM forecast and the ECMWF-initialized analysis field at 1200 UTC 13 January. Solid (dashed) lines correspond to positive (negative) values (spacing 1 PVU, zero line omitted). (b) The backward traced envelope of the upper-level PV anomaly labeled P_1 in Fig. 5. The envelope is indicated by a dashed line at 1200 UTC 13 January, a dotted line at 0000 UTC 13 January, and a continuous line at 1200 UTC 12 January. (c) The analog of (b) but for the envelope of the upper-level PV anomaly labeled P_3.

trodicted for four successive intervals of 6 h to 1200 UTC 12 January. At the end of each interval the modified PV distribution is inverted to derive a revised estimate of the flow. Depictions of the initial location and subsequent track of the two envelopes on the 310-K surface are shown in Figs. 10b,c. The P_1-related and the P_3-related anomalies at 1200 UTC 12 January have the form of two elongated bands that extend out over the Atlantic from near Newfoundland.

The result of step 3—the reconstitution of the fields at 1200 UTC 12 January—is shown in Fig. 11. Comparison with the corresponding analyzed patterns for this time (Fig. 3) is instructive. On the 310-K isentropic surface, the PV pattern is more richly structured with a stronger PV streamer extending southeast from Newfoundland into the Atlantic and a localized anomaly located poleward of its tip and within the stratospheric reservoir. In contrast, at 850 hPa, the meteorological fields are essentially unchanged and this is consistent (see next subsection) with the signal from the upper-level mesoscale PV anomalies having a short vertical penetration scale.

The result of step 4—the 24-h forecast starting from the modified initial state at l200 UTC 12 January—yields the forecast displayed in Figs. 12–14. Comparison with the corresponding ECMWF fields (Figs. 3–5) show that the structure of the upper-level PV pattern bears a closer resemblance to their analysis. However, the P_1 anomaly is more fragmented and assumes a structure not unlike the P_1–P_2 couplet in the analysis field. (We comment further on this aspect in the next subsection.) At low levels the features resemble the realized cyclone, and in particular the observed and ''repredicted'' low-level PV anomalies possess similar structures and amplitude.

Figure 15 shows the track and pressure fall of the surface wave cyclone as recorded in the analysis and as predicted in the original and the revised forecasts. In the revised forecast the cyclone follows the observed track but fails to capture the full pressure drop during the last 6 h of the integration.

d. Discussion

This case study demonstrates the feasibility and the potential of the present diagnostic approach for analyzing misforecasts. To further illustrate this point we consider here four aspects that arise directly from an in-

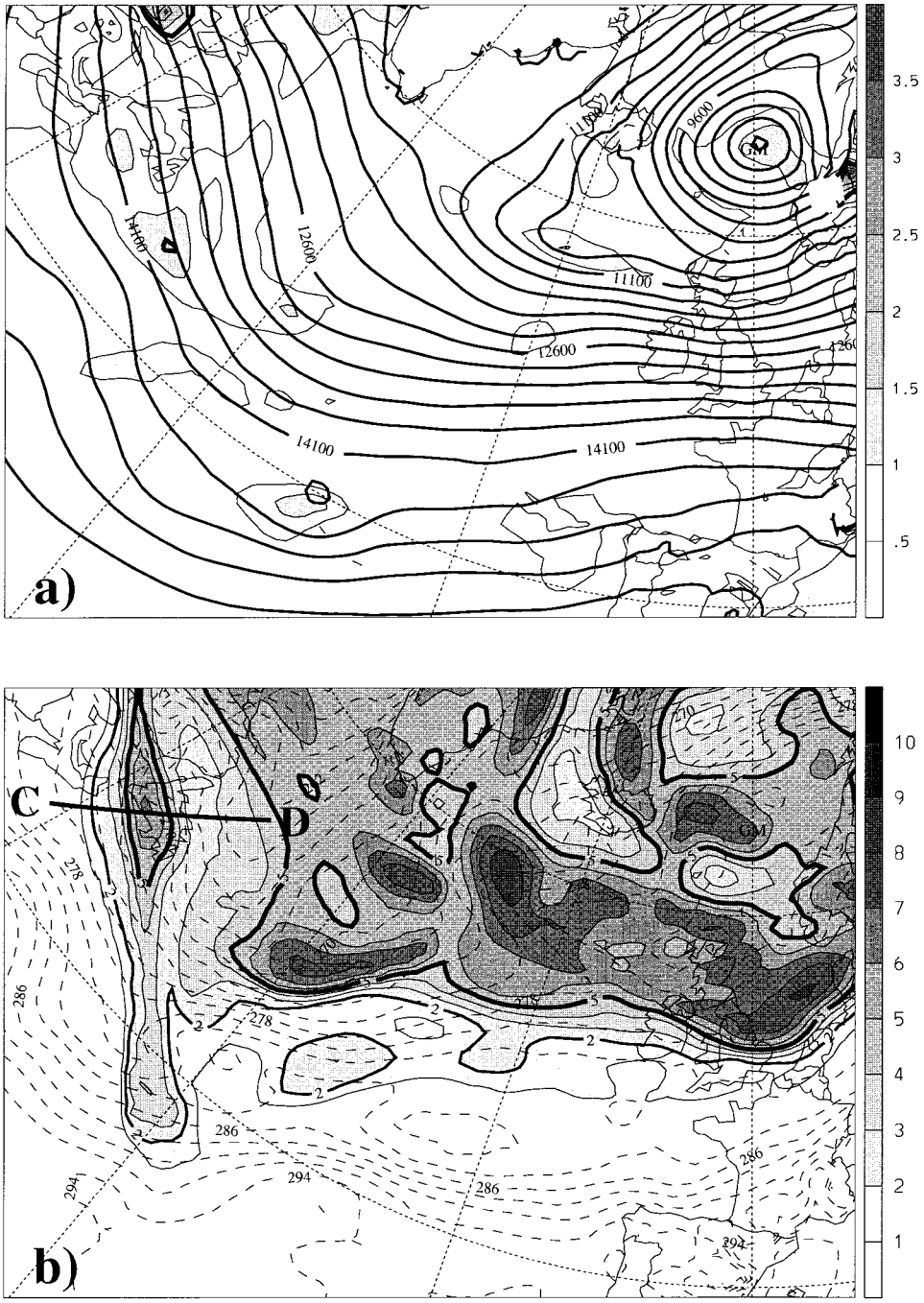

FIG. 11. Revised initial fields that incorporate the two retrodicted PV anomalies P_1 and P_3. (Displayed fields and spacings as in Fig. 3.)

tercomparison of the ECMWF analysis, the original EM forecast, and the revised forecast with the modified initial state.

First, consider the original and the revised forecasts. The significant difference between these fields lends credence to the hypothesis that subsynoptic–mesoscale upper-level PV anomalies can exert a seminal influence upon surface wave cyclogenesis. Furthermore, it indicates that the present approach constitutes an attractive tool for examining predictability aspects of such systems. (As an aside, we stress that the role of the upper-level anomalies might be merely catalytic and possibly confined to triggering or modifying the location, timing, or amplitude of the low-level convection. It is clear that

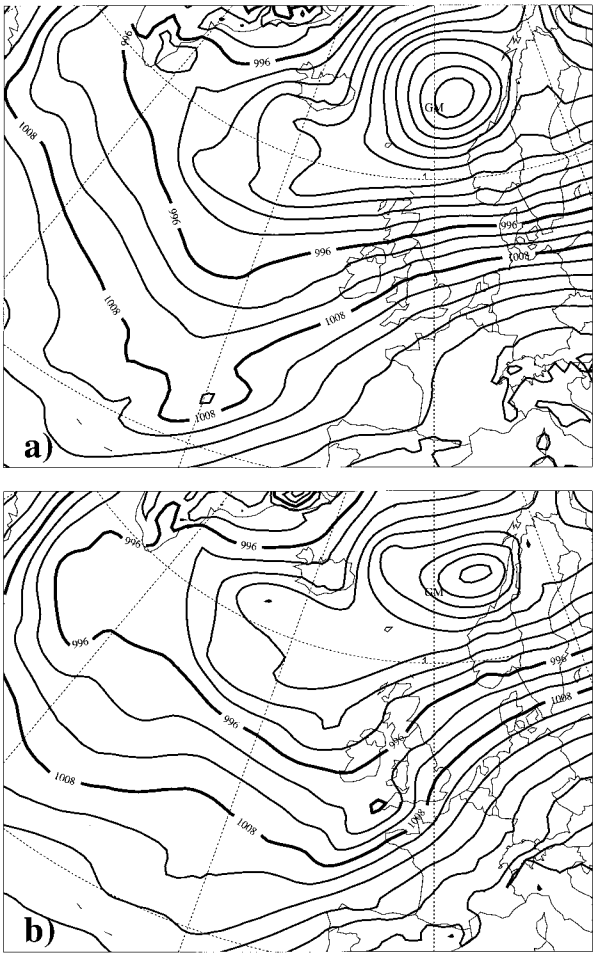

FIG. 12. As for Fig. 2 but now derived from the revised forecast.

the strong low-level PV signature of this cyclogenesis event is diabatically induced in situ.)

Second, consider the upper-level PV anomalies in the ECMWF analysis and in the revised analysis at the initial time. The difference in their structure, together with the comparative success of the ''revised forecast,'' suggests that this difference accounts for a significant component of the error in the initial state. The retrodicted ''PV errors'' are finescaled and located near the tropopause break and jet stream(s). These factors render their signal less apparent in the in situ geopotential and thermal fields. For example, it is difficult to visually distinguish between the 300-hPa geopotential patterns of the ECMWF and the revised analyses, and the quantitative difference amounts to a maximum of about 50 m at the core of the trough. The signal associated with the P_1 anomaly can be inferred from Fig. 16. The figure shows features of the ECMWF and the revised analysis at 1200 UTC 12 January in a vertical section aligned across the distinctive PV filament extending out over the Atlantic. The retrodicted P_1 anomaly directly supplements and intensifies the potential vorticity of this filament, concomitantly reduces (strengthens) by some 10 m s^{-1} the jet stream located to its west (east), and modifies somewhat more weakly the potential temperature field. The vertical penetration of this subsynoptic anomaly is comparatively small and its signal is not apparent below 700 hPa. One inference is that the anomaly's detection is favored by in situ wind measurements.

Third, consider the structure of the analyzed surface event and that simulated in the revised forecast. The reasonable resemblance suggests that the dynamics of the PV anomalies detected at upper-level relate directly to and can shed light upon the nature of the error evolution. In this context consider the dynamics of the two anomalies P_1 and P_3. From a PV perspective their interaction influences their tracks. For example, it induces a tendency to increase the eastward progression of P_1 and to decrease that of P_3. This inference is supported, for example, by the velocity signal of the P_1 anomaly as deduced from Fig. 16. Likewise, P_1 and P_3 can in principle influence the movement and development of the surface low. The evidence of Fig. 16 suggests that, at least initially, the influence upon the track is negligible. However, the anomaly P_1 is suitably located to influence the location and strength of the low-level ascent and thereby to instigate and maintain the diabatic processes responsible for the generation of the PV tower.

Further insight, and indeed support, for the foregoing inferences can be gained by applying the method set out in section 2 in slightly different forms. Here we record some examples: (a) a simulation based upon the prior retrodiction of only the single anomaly P_1 produced, in comparison with the earlier ''standard'' experiment, a surface low with a similar structure but a retarded location; (b) a simulation following the retrodiction of a large upper-level envelope encompassing all three anomalies (P_1, P_2, and P_3) resulted in only a marginally better forecast; and (c) a repeat of the standard simulation but omitting the intermittent PV inversions during the retrodiction (i.e., performing the backward integration with merely the analyzed fields) resulted in a significant misplacement of the cyclone. The latter experiment serves to illustrate the nonlinearity of the error evolution.

Fourth, consider the structure of the upper-level PV anomalies of the revised forecast and the ECMWF analysis at the final forecast time (Figs. 5b and 14b). It was noted earlier that the revised forecast resulted in a more fragmented P_1 anomaly. This is partly attributable to the revised forecast being based only upon a retrodiction of P_1 and P_3. Other factors contributing to the difference are one or a combination of the following factors: (i) observational error at the forecast time, (ii) errors arising from numerical and/or physical limitations of the forecast model during the revised forecast, (iii) errors deriving from the four-step diagnostic procedure (in particular the approximations associated with the trajec-

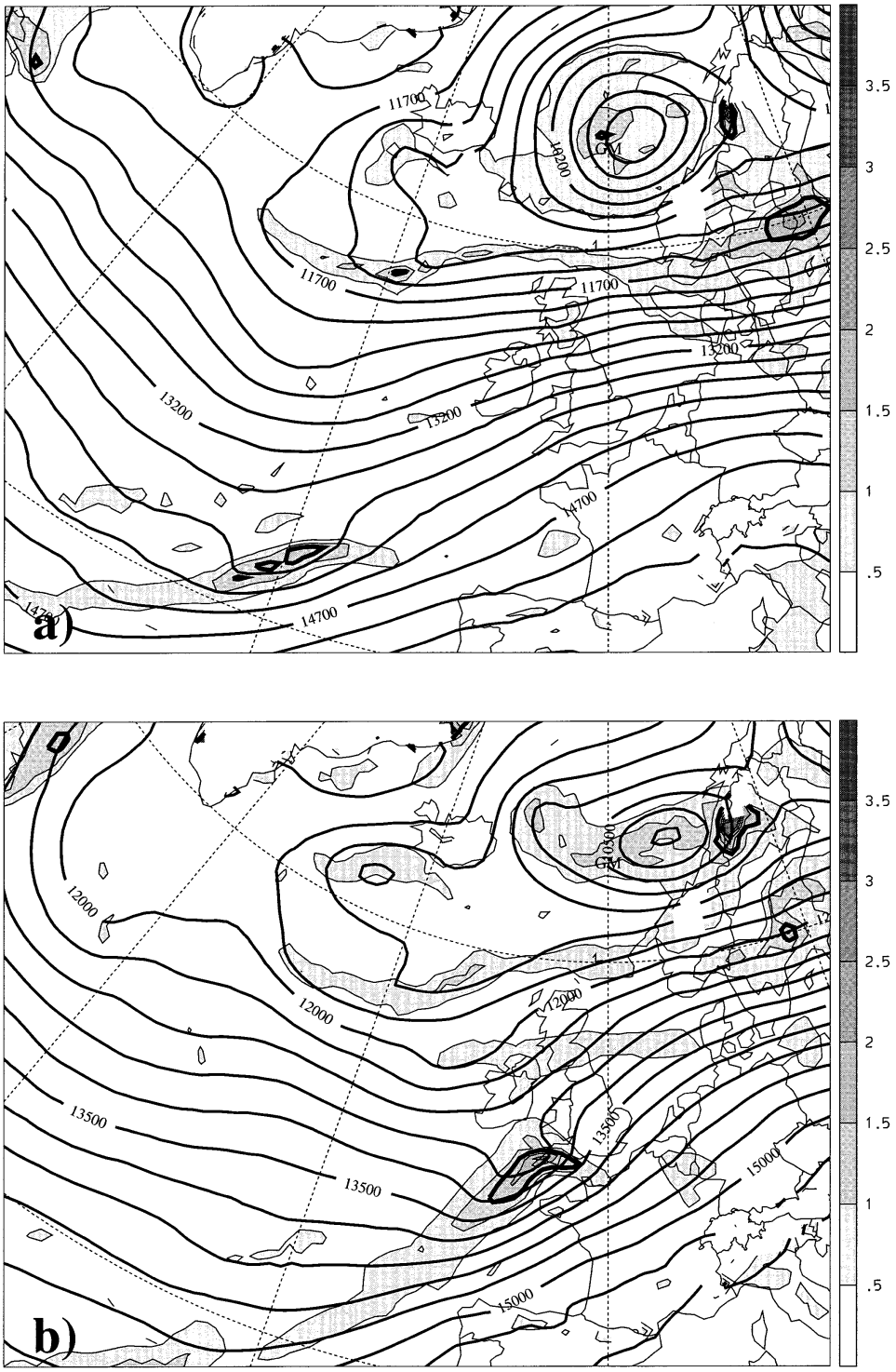

FIG. 13. The analog of Fig. 4 but for the revised forecast.

tories and the form adopted for the PV inversion), and (iv) the incomplete representation of the upper–lower-level interactions during retrodiction. None of these factors can be excluded a priori, and their relative contributions are difficult to disentangle since they are coupled during the retrodiction and forecast. The first three factors are in effect technical limitations. The fourth is intrinsic and related to the irreversibility of diabatic and/or rapidly mixing flow, and fragmentation of a PV anomaly is one phase of such mixing.

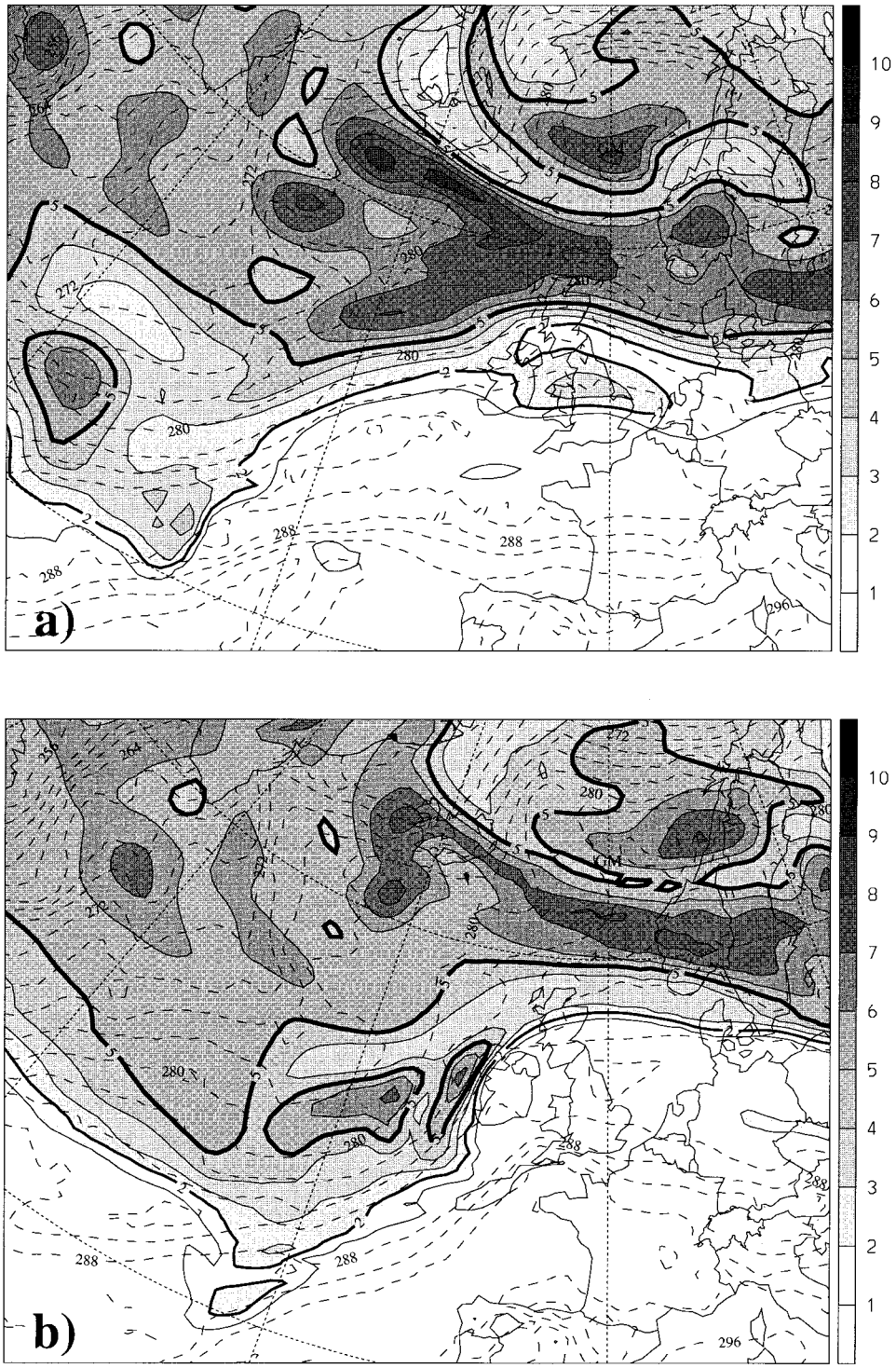

FIG. 14. The analog of Fig. 5 but for the revised forecast.

4. Further remarks

In essence this study indicates that our phenomenological approach is useful for the diagnosis of misforecasts associated with upper-level errors. The adoption of a PV perspective helps to locate the geographical domain of the initial error and provides dynamical insight on the nature of the space–time evolution of that error. In principle, the approach can also shed light on some esoteric aspects of predictability and on practical strategies for remeding deficiencies in the analysis.

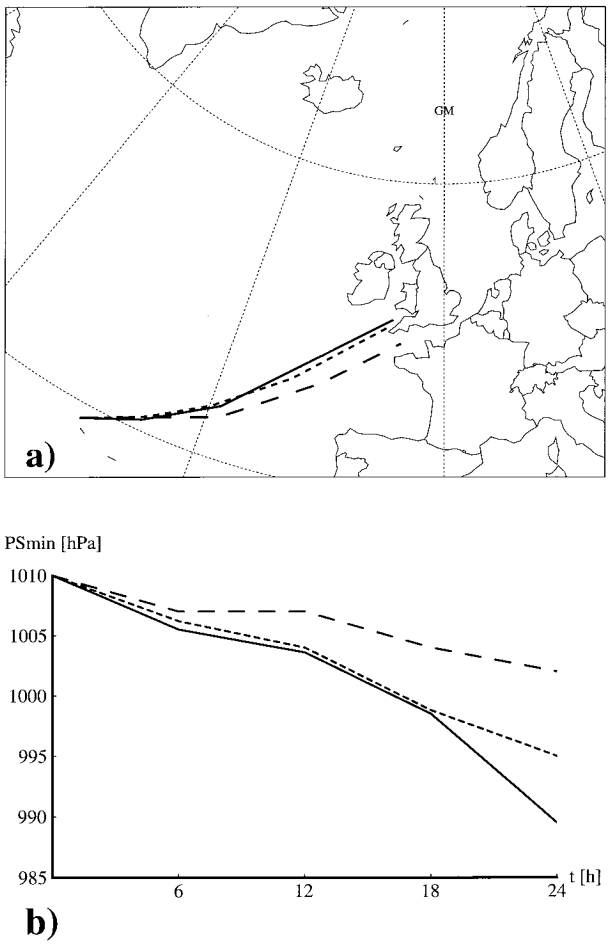

FIG. 15. (a) The track of the cyclone and (b) the minimum sea surface pressure. The solid lines correspond to the ECMWF analysis fields, long-dashed lines to the standard EM forecast, and short-dashed ones to the revised forecast.

In the context of predictability, we first note that singular vector analysis of idealized simulations of cyclogenesis (Rabier et al. 1992; Langland et al. 1995) and routine ensemble predictions (Molteni et al. 1996) both indicate that the amplitude of the dominant singular vectors tend to be confined to the lower troposphere. An interpretation is that suitably located small PV perturbations at these elevations can rapidly induce large-amplitude signals in the potential vorticity pattern at tropopause level and in the potential temperature pattern at the surface and that thereafter these induced perturbations could interact synergetically [cf. the quasi-resonant growth documented for an idealized, but related configuration, by Davies and Bishop (1994)]. Whereas such mechanism might set the intrinsic predictability limit for initially *linear* atmospheric perturbations, the preexistence of *finite-amplitude* perturbations at tropopause level in realized flows can eliminate the need for, and reliance upon, a low-troposphere perturbation.

The diagnostic approach advocated in this study also has import for the design of adaptive observational strategies. This follows from noting that tropopause-level PV errors can influence the flow field throughout the troposphere, whereas their correction requires only in situ data. In effect, for these forms of error, additional data would be required only in a domain that is limited both horizontally and vertically.

Information related to the location of such domains can be obtained by (a) routine use of the approach to yield climatological statistics on the frequency and location of PV errors and (b) quasi-real-time inspection of the upper-level PV errors plus frequent retrodictions (of, say, 12 h) to provide synoptic patterns of the ''current'' error.

Improvement of the analysis fields within the presumed error domain can be sought by a more effective use of the time history of the available data and possibly from appropriate adaptive observational strategies. It is helpful to note that the existence and evolution of tropopause-level flow features that are seminal to surface development are evident in satellite water vapor images (see, e.g., Appenzeller et al. 1996). For the case study reported here we also note that the domain of the initial error is regularly traversed by intercontinental flights of commercial airlines and that upstream over the North American continent there is also a wealth of observational data. However, the efficacy of the latter data is diminished somewhat by the potentially rapid evolution of the upper-level anomalies.

Finally we note that there have been two recent approaches to ameliorating the deficiencies in the initial fields, and both hinge upon the rapid identification of the evolving error fields and the instigation of corrective measures. Rabier et al. (1996) extended their study of the sensitivity of errors in the forecast field to the initial analysis and demonstrated that there is a potential to derive improved forecasts by performing a revised and longer forecast with a suitably modified initial field. M. Demirtas and A. Thorpe (1996 private communication) advocate monitoring the satellite water vapor imagery and, in the event of a mismatch with the model's initial analysis, adjusting the analyzed tropopause's topography to align with the imagery. In a similar vein to these studies, the present approach could also be adapted to provide ongoing pseudo-forecasts by regularly performing short (6 or 12 h) cycles of ''forecast–analysis–retrodiction,'' followed by an extended revised forecast.

Acknowledgments. We are indebted to the German Weather Service and the Swiss Meteorological Institute for providing access to the EM model. It is also a pleasure to thank Drs. Daniel Lüthi and Heini Wernli for being ever-ready in their help and support.

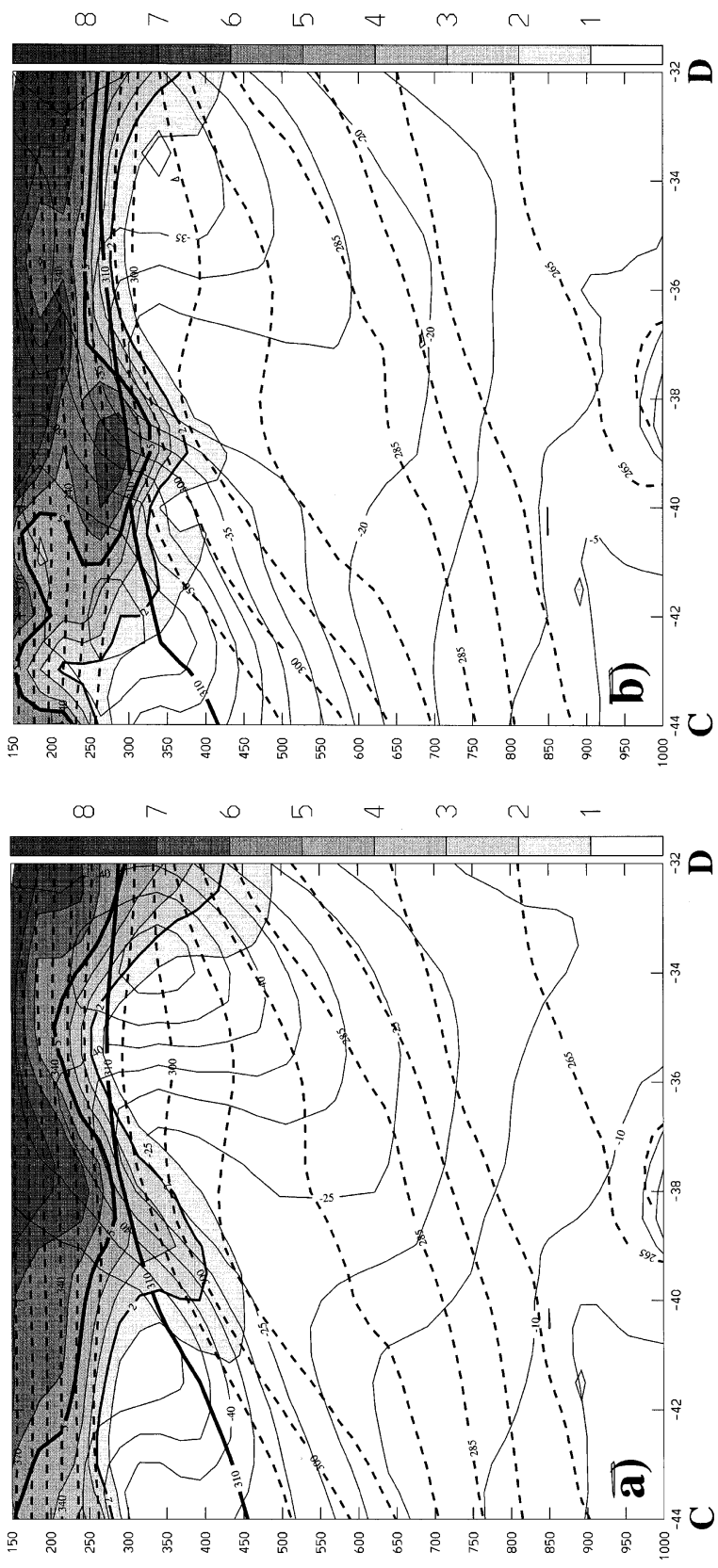

FIG. 16. Cross sections at 1200 UTC 12 January along the line labeled CD in Figs. 3 and 11. The section transects the PV filament extending from the western Atlantic seaboard and are derived from (a) the ECMWF initialized analysis and (b) the initial state for the revised forecast. The displayed fields are PV (shaded, spacing 1 PVU, the thick line corresponds to the 2-PVU and the bold to the 5-PVU isoline), potential temperature (dashed lines, thick line indicates 310 K, spacing 5 K for values less than or equal to 310 K and 10 K for values greater than 310 K), and cross-velocity field (thin lines, spacing 5 m s^{-1}).

REFERENCES

Appenzeller, C., and H. C. Davies, 1992: Structure of stratospheric intrusions into the troposphere. *Nature*, **358,** 570–572.

——, and ——, 1996: PV morphology of a frontal-wave development. *Meteor. Atmos. Phys.*, **58,** 21–40.

——, ——, and W. A. Norton, 1996: Fragmentation of stratospheric intrusions. *J. Geophys. Res.*, **101**(D1), 1435–1456.

Browning, K. A., and N. M. Roberts, 1994: Structure of a frontal cyclone. *Quart. J. Roy. Meteor. Soc.*, **120,** 1535–1557.

Davies, H. C., and C. H. Bishop, 1994: Eady edge waves and rapid development. *J. Atmos. Sci.*, **51,** 1930–1946.

Davis, C. A., and K. A. Emanuel, 1991: Potential vorticity diagnostic of cyclogenesis. *Mon. Wea. Rev.*, **119,** 1929–1953.

Ehrendorfer, M., and R. M. Errico, 1995: Mesoscale predictability and the spectrum of optimal perturbations. *J. Atmos. Sci.,* **52,** 3475–3500.

Errico, R. M., and D. P. Baumhefner, 1987: Predictability experiments using a high-resolution limited-area model. *Mon. Wea. Rev.*, **115,** 408–504.

——, and T. Vukicevic, 1992: Sensitivity analysis using an adjoint of the PSU–NCAR Mesoscale Model. *Mon. Wea. Rev.*, **120,** 1644–1660.

——, ——, and K. Raeder, 1993: Comparison of initial and lateral boundary condition sensitivity for a limited-area model. *Tellus*, **45A,** 539–557.

Gyakum, J. R., and Coauthors, 1995: First COMPARE Workshop: 5–9 October 1994, Montreal, Quebec, Canada. *Bull. Amer. Meteor. Soc.*, **76,** 1209–1218.

Hoskins, B., and P. Berrisford, 1988: A potential vorticity perspective of the storm of 15–16 October 1987. *Weather*, **43,** 122–129.

——, M. E. McIntyre, and A. W. Robertson, 1985: On the use and significance of isentropic potential vorticity maps. *Quart. J. Roy. Meteor. Soc.*, **111,** 877–946.

Joly, A., and A. J. Thorpe, 1990: Frontal instability generated by tropospheric potential vorticity anomalies. *Quart. J. Roy. Meteor. Soc.*, **116,** 525–560.

Kuo, Y.-H., and R. J. Reed, 1988: Numerical simulations of an explosively deepening cyclone in the eastern Atlantic. *Mon. Wea. Rev.*, **116,** 2081–2105.

Langland, R. H., R. L. Elsberry, and R. M. Errico, 1995: Evaluation of physical processes in an idealized extratropical cyclone using adjoint sensitivity. *Quart. J. Roy. Meteor. Soc.*, **121,** 1349–1386.

Lüthi, D., C. Frei, C. Schär, and H. C. Davies, 1996: A regional climate model for the Alpine region. NFP 31 Publ., Vdf. Hochschulverlag, 53 pp.

Majewski, D., 1991: The Europa-Modell of the Deutscher Wetterdienst. *Numerical Methods in Atmospheric Models*, Vol. 2, European Centre for Medium-Range Weather Forecasts, 147–191.

Malardel, S., A. Joly, F. Courbet, and P. Courtier, 1993: Nonlinear evolution of ordinary frontal waves induced by low-level potential vorticity anomalies. *Quart. J. Roy. Meteor. Soc.*, **119,** 681–713.

Molteni, F., R. Buizza, T. N. Palmer, and T. Petroliagis, 1996: The ECMWF ensemble prediction system: Methodology and validation. *Quart. J. Roy. Meteor. Soc.*, **122,** 73–120.

Mullen, S. L., and D. L. Baumhefner, 1989: The impact of initial condition uncertainty on numerical simulations of large-scale explosive cyclogenesis. *Mon. Wea. Rev.*, **117,** 2800–2821.

Rabier, R., P. Courtier, and O. Talagrand, 1992: An application of adjoint models to sensitivity analysis. *Beitr. Phys. Atmos.*, **65,** 177–192.

——, E. Klinker, P. Courtier, and A. Hollingsworth, 1996: Sensitivity of forecast errors to initial conditions. *Quart. J. Roy. Meteor. Soc.*, **122,** 121–150.

Reed, R. J., and M. T. Stoelinga, 1992: A model-aided study of the origin and evolution of the anomalously high potential vorticity in the inner region of a rapidly deepening marine cyclone. *Mon. Wea. Rev.*, **120,** 893–913.

Schär, C., and H. C. Davies, 1990: An instability of mature cold fronts. *J. Atmos. Sci.*, **47,** 929–950.

Shutts, G. J., 1990: Dynamical aspects of the October Storm 1987: A study of a successful fine-mesh model simulation. *Quart. J. Roy. Meteor. Soc.*, **116,** 1315–1347.

Simmons, A. J., 1991: Development of a high resolution, semi-Lagrangian version of the ECMWF forecast model. *Numerical Methods in Atmospheric Models*, Vol. 2, European Centre for Medium-Range Weather Forecasts, 281–324.

——, R. Mureau, and T. Petroliagis, 1995: Error growth and estimates of predictability from the ECMWF forecasting system. *Quart. J. Roy. Meteor. Soc.*, **121,** 1739–1771.

Thorncroft, C. D., and B. J. Hoskins, 1990: Frontal cyclogenesis. *J. Atmos. Sci.*, **47,** 2317–2336.

van Tuyl, A. H., and R. M. Errico, 1989: Scale interaction and predictability in a mesoscale model. *Mon. Wea. Rev.*, **117,** 495–517.

Vukicevic, T., 1991: Nonlinear and linear evolution of initial forecast errors. *Mon. Wea. Rev.*, **119,** 1602–1611.

Wernli, H., and H. C. Davies, 1997: A Lagrangian-based analysis of extratropical cyclones. Part I: The method and some applications. *Quart. J. Roy. Meteor. Soc.*, in press.